

Selective Hydrogenation of Biomass-Derived Furfural: Enhanced Catalytic Performance of Pd–Cu Alloy Nanoparticles in Porous Polymer

Ksenia E. Salnikova,^[a, b] Yurii V. Larichev,^[c, d] Esther M. Sulman,^[a] Alexey V. Bykov,^[a] Alexander I. Sidorov,^[a] Galina N. Demidenko,^[a] Mikhail G. Sulman,^[a] Lyudmila M. Bronstein,^{*,[e, f, g]} and Valentina G. Matveeva^{*,[a, b]}

Here, the development of a new catalyst is reported for the selective furfural (FF) hydrogenation to furfuryl alcohol (FA) based on about 7 nm sized Pd–Cu alloy nanoparticles (NPs) formed in inexpensive, commercially available micro/mesoporous hypercrosslinked polystyrene (HPS). A comparison of the catalytic properties of as-synthesized and reduced (denoted “r”) catalysts as well as Pd–Cu alloy and monometallic palladium NPs showed a considerable enhancement of the catalytic performance of Pd–Cu/HPS-r compared to other catalysts

studied, resulting in about 100% FF conversion, 95.2% selectivity for FA and a TOF of 1209 h⁻¹. This was attributed to the enrichment of the NP surface with copper atoms, disrupting the furan ring adsorption, and to the presence of both zerovalent and cationic palladium and copper species, resulting in optimal hydrogen and FF adsorption. These factors along with exceptional stability of the catalyst in ten consecutive catalytic cycles make it highly promising in practical applications.

Introduction

In recent years, a great deal of attention has been paid to the development of environmentally friendly processes using biomass ingredients as precursors for syntheses of value-added chemicals. Furfural (FF) is a high-output chemical obtained by dehydration of xylose (a byproduct of farming and wood

processing)^[1] and utilized for hydrogenation to furfuryl alcohol (FA), tetrahydrofurfuryl alcohol (THFA), cyclopentanone, etc.^[2] FA is generally used in a paint production, as solvent and precursor in the production of glass fiber and polymer concrete.^[3] Heterogeneous catalysts are commonly employed in the FF hydrogenation due to their high stability, facile separation from the reaction medium, and recyclability.^[4]

The most frequently utilized noble metal catalysts in FF hydrogenation are based on Pd nanoparticles (NPs) stabilized by various supports^[5] such as carbons (non-modified and chemically modified)^[6] and metal oxides (SiO₂, Al₂O₃, MgAl oxides, etc.), including mesoporous solids and those modified with transition metals (Ti, Zr, Sn).^[2b,6b] The support can control the interactions between the metal surface and the furan ring, thus, controlling selectivity. Pd NPs formed on amorphous supports (SiO₂, Al₂O₃) were found to be quite efficient for the FF hydrogenation, while doped ordered mesoporous supports (TiMCM-41, ZrMCM-41, SnMCM-41) allowed for higher selectivity to FA and THFA.^[2b] Moreover, Pd NPs placed in mesopores were more stable than those on the support surface, allowing higher reusability. The support porosity is definitely advantageous for catalysis, but commercially available mesoporous silica and alumina have low attrition resistance which jeopardizes the catalyst stability.^[7]

Porous crosslinked polymers have shown multiple advantages as catalyst supports, including controlled porosity and a high tensile strength, i.e., enhanced attrition resistance.^[8] In our preceding work, Pd NPs were formed in commercially available micro/mesoporous hypercrosslinked polystyrene (HPS) using two different precursors, PdCl₂(CH₃CN)₂ and Pd(CH₃COO)₂, and studied in FF hydrogenation to FA.^[2a] It was shown that FF conversion and selectivity to FA were higher for smaller Pd NPs, but no other structural features were explored.

[a] K. E. Salnikova, Prof. E. M. Sulman, Dr. A. V. Bykov, Dr. A. I. Sidorov, Dr. G. N. Demidenko, Prof. M. G. Sulman, Prof. V. G. Matveeva
Department of Biotechnology and Chemistry
Tver State Technical University
A.Nikitin str., 22, 170026 Tver (Russia)
E-mail: matveeva@science.tver.ru

[b] K. E. Salnikova, Prof. V. G. Matveeva
Regional technological centre
Tver State University
Zhelyabova str., 33, 170100 Tver (Russia)


[c] Dr. Y. V. Larichev
Boreskov Institute of Catalysis
5 Academician Lavrentiev Avenue, 630090 Novosibirsk (Russia)

[d] Dr. Y. V. Larichev
Novosibirsk State University
2 Pirogov Street, 630090 Novosibirsk (Russia)

[e] Dr. L. M. Bronstein
Department of Chemistry
Indiana University
800 E. Kirkwood Av., Bloomington, IN, 47408 (USA)
E-mail: lybronst@indiana.edu

[f] Dr. L. M. Bronstein
A.N. Nesmeyanov Institute of Organoelement Compounds
Russian Academy of Sciences
28 Vavilov St., Moscow 119991 (Russia)

[g] Dr. L. M. Bronstein
Faculty of Science
Department of Physics
King Abdulaziz University
Jeddah 21589 (Saudi Arabia)

 Supporting information for this article is available on the WWW under <https://doi.org/10.1002/cplu.202000383>

It is well-established that modification of Pd NPs with a second metal is an excellent way to control a reaction pathway and selectivity in the FF hydrogenation via weakening the H₂ adsorption on Pd and altering the FF adsorption.^[9] Poisoning of Pd with Bi allowed the FF hydrogenation with a high selectivity to FA and cyclopentanone.^[9d] It is believed that in the Pd–Bi catalyst there is an active site isolation, which is accountable for the increase of selectivity to target products, while eliminating oligomeric byproducts. Copper is another metal of choice for Pd NP modification.^[1a,4a,c,5a,6c,9c,10] Alloying of Pd and Cu leads to higher reactivity.^[6c,9c] In the case of Cu@Pd core-shell bimetallic catalysts, it was demonstrated that an enhanced activity can be assigned to decreased hydrogen surface coverage, making more catalytic sites accessible for FF adsorption.^[1a]

Taking into account successes of Pd–Cu alloys in the FF hydrogenation to FA and advantages of the micro/mesoporous HPS support in a number of hydrogenation reactions,^[11] in this work we developed novel heterogeneous catalysts with Pd–Cu alloy NPs in the HPS pores and compared their properties with

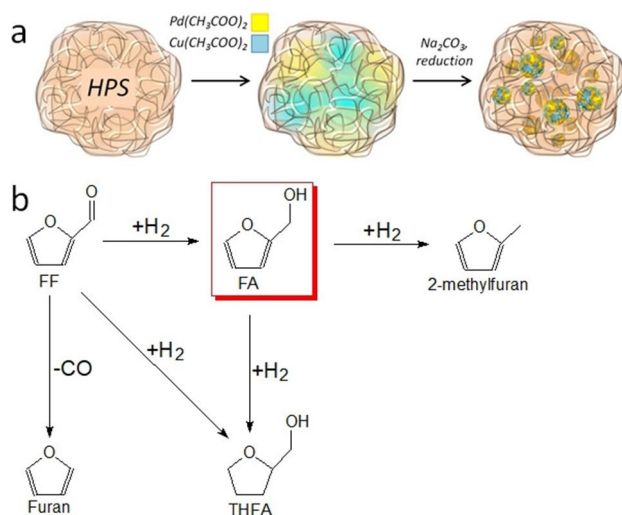
those of monometallic Pd NPs. We demonstrate that the formation of Pd–Cu alloy NPs, whose surface is enriched with Cu atoms and contains a fraction of cationic Pd and Cu species, leads to high FF conversion and FA selectivity as well as an enhanced activity and reusability.

Results and Discussion

Catalytic properties

The catalyst synthesis was carried out by impregnation of HPS with the solution containing both palladium and copper acetates, followed by the Na₂CO₃ treatment to precipitate NPs in the HPS pores (Scheme 1a). This results in the formation of mixed Pd–Cu oxides as reported elsewhere.^[12] These as-synthesized samples are denoted “as”. The reduction of Pd and Cu species was performed prior to the catalytic reaction in the hydrogen flow at 275 °C. The reduced samples are denoted “r”. The Pd and Cu contents in the catalysts were varied between 1 and 5 wt.% by loading, keeping the Pd:Cu molar ratio unchanged at 1:1.7 (Table 1). The molar ratio was varied for the catalysts containing 1 and 5 wt.% of Pd or Cu. The elemental analysis data for key samples are presented in Table S1 in the Supporting Information.

Before studying catalytic properties of bimetallic Pd–Cu/HPS catalysts in the FF hydrogenation, we tested monometallic Cu/HPS and Pd/HPS catalysts synthesized in a similar way. The data presented in Table S2 demonstrate that although Cu catalyzes the FF hydrogenation, the conversion is low and the main products are furan and 2-methylfuran (Scheme 1b) with no selectivity to any product. This was surprising considering high selectivity and conversion of Cu-containing catalysts on metal oxide supports^[10] and could be tentatively attributed to the HPS influence. For Pd/HPS catalysts (Table S2), the conversion increases with the increase of the Pd content and for all the samples, two products are observed: FA and THFA. The best selectivity to FA was obtained for the catalyst containing 3 wt.% of Pd. Moreover, for all the samples, both conversion and selectivity are higher for the catalysts where Pd-containing NPs



Scheme 1. Schematic representation of the formation of Pd–Cu NPs in the HPS pores (a) and FF hydrogenation (b). The red rectangle in (b) shows the target product, FA.

Table 1. Catalytic properties of Pd–Cu bimetallic catalysts in the FF hydrogenation.^[a]

| Catalyst | Pd/Cu, wt.% [by XRF] | Molar ratio, Pd:Cu | FF conversion, % | Selectivity, % | | | |
|-----------------|----------------------|--------------------|------------------|----------------|------|-------|----------------|
| | | | | FA | THFA | Furan | 2-methyl-furan |
| Pd–Cu/HPS-as | 3/3 | 1:1.7 | 88.5 | 86.2 | 7.7 | 2.3 | 3.8 |
| Pd–Cu/HPS-r | 3/3 | 1:1.7 | 99.9 | 95.2 | 3.2 | 1.1 | 0.5 |
| Pd–Cu/HPS(1)-as | 1/1 | 1:1.7 | 69.2 | 76.2 | 11.2 | 7.4 | 5.2 |
| Pd–Cu/HPS(1)-r | 1/1 | 1:1.7 | 78.4 | 78.5 | 13.8 | 4.1 | 3.6 |
| Pd–Cu/HPS(2)-as | 5/5 | 1:1.7 | 94.9 | 77.2 | 12.7 | 5.4 | 4.7 |
| Pd–Cu/HPS(2)-r | 5/5 | 1:1.7 | 99.9 | 87.3 | 8.5 | 2.3 | 1.9 |
| Pd–Cu/HPS(3)-as | 1/5 | 1:8.4 | 66.2 | 67.9 | 8.9 | 13.2 | 10.0 |
| Pd–Cu/HPS(3)-r | 1/5 | 1:8.4 | 75.5 | 73.3 | 10.2 | 7.7 | 8.8 |
| Pd–Cu/HPS(4)-as | 5/1 | 1:0.33 | 96.5 | 61.6 | 20.3 | 10.5 | 7.6 |
| Pd–Cu/HPS(4)-r | 5/1 | 1:0.33 | 98.2 | 79.2 | 15.6 | 3.3 | 1.9 |
| Pd/HPS-as | 3/0 | – | 63.9 | 74.2 | 25.8 | – | – |
| Pd/HPS-r | 3/0 | – | 79.9 | 84.6 | 15.4 | – | – |

[a] Reaction conditions: temperature 120 °C, pressure (H₂) 6 MPa, furfural volume 2 mL, isopropanol volume 48 mL, catalyst amount 0.1 g, reaction time 180 min.

were reduced by hydrogen vs. as-synthesized catalysts, whose oxidized Pd species were reduced *in situ* during the catalyst activation and the catalytic reaction.

For bimetallic catalysts with the Pd:Cu=1:1.7 molar ratio (Table 1), the increase of the metal loading leads to the FF conversion increase for both as-synthesized and reduced catalysts. The maximum FF conversion of 99.9% is achieved for reduced catalysts containing 3 or 5 wt.% of each metal. At the same time, the selectivity varies. For all bimetallic catalysts, furan and 2-methylfuran are present in the reaction mixture due to the presence of Cu (Table S2). The best selectivity to FA (95.2%) is obtained for 3 wt.% of metal loading, while at the higher content (5 wt.%) the selectivity to FA drops to 87.3% due to the increased THFA amount, indicating an acceleration of the C=C hydrogenation of the furan ring. An increase or decrease of the Pd:Cu molar ratio to 1:0.33 or 1:8.4 (Pd:Cu weight ratios of 5:1 and 1:5, Table 1) results in the decrease of the selectivity to FA and the increase of fractions of other compounds: THFA, furan, and 2-methylfuran.

Thus, the best conversion (99.9%) and selectivity (95.2%) were obtained for the reduced Pd–Cu catalyst containing 3 wt.% of each metal. For this catalyst, a carbon balance was calculated using an overall carbon yield to verify fidelity of the product analysis.^[13] The overall carbon yield (%) expressed as $(5 \times C_5 \text{ moles} + 4 \times C_4 \text{ moles})_{\text{products}} / (5 \times C_5 \text{ moles})_{\text{FF}} \times 100\%$ is equal 99.78%. Taking into account cleavage of CO (not measured) upon the furan formation, the total carbon yield is 100%.

Monometallic Pd/HPS-r with the same Pd content showed much lower conversion (79.9%) and selectivity (84.6%) than those for Pd–Cu/HPS-r.

Influence of FF hydrogenation conditions on catalysis

The dependencies of the conversion and selectivity on time, hydrogen pressure, and the reaction temperature for Pd/HPS and Pd–Cu/HPS samples with 3 wt.% of each metal loading (Table S1) are presented in Figure 1. The data show that for all the samples, the highest conversion is achieved for 180 min and at the 6 MPa hydrogen pressure, while the temperatures for reaching the highest conversion differ. For Pd–Cu/HPS-r, it is already reached at 120 °C, while for three other samples, a higher temperature (140 °C) is needed. As for selectivity, the highest value is obtained at the beginning of the reaction which is consistent with literature data.^[14] For Pd–Cu–HPS-r, the selectivity remains nearly unchanged until the end of the reaction, while for other samples, it noticeably drops. For all samples, the selectivity is the highest at 6 MPa pressure and 120 °C, which determined our choice of optimal reaction conditions. It is noteworthy that in all reaction conditions, the conversion and selectivity are higher for Pd–Cu bimetallic catalysts compared to Pd/HPS.

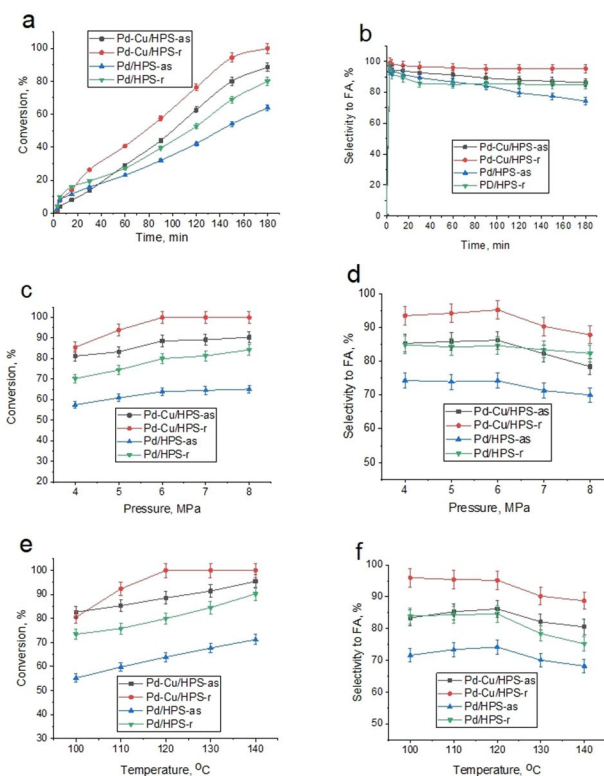


Figure 1. Dependencies of the conversion (a,c,e) and selectivity (b,d,f) on time (a,b), pressure (c,d), and temperature (e,f).

Structure, morphology, and textural properties

To better understand the influence of the synthetic procedure (prior to reduction) and the Cu presence on the behavior of bimetallic Pd–Cu/HPS catalysts, we studied structure, morphology, and textural properties of four Pd–Cu/HPS and Pd/HPS samples listed in Table S2.

Porosity data for bimetallic Pd–Cu and monometallic Pd samples are presented in Table S3 and Figure S1 in the Supporting Information. Liquid nitrogen adsorption-desorption isotherms (Figure S1a,b) are typical for micro-mesoporous hypercrosslinked polymers.^[15] The changes in surface areas and pore volumes (Table S3) show a similar trend for HPS samples with both bimetallic and monometallic NPs: upon precipitation of NPs in the HPS pores (as-synthesized samples), the polymer porosity decreases and then further decreases upon the NP reduction. The size of the majority of mesopores (4 nm) remains unchanged but their pore volume significantly decreases after NP incorporation. Larger mesopores with diameters in the range of 4–20 nm display a similar behavior. These data indicate that NPs are formed in the pores, leading to the decrease of the pore volume and pore surface area, however, they are not blocking pore junctions because the porosity decrease is moderate.

To evaluate NP sizes, we used small-angle X-ray scattering (SAXS) and transmission electron microscopy (TEM). It is noteworthy that for NP-containing HPS samples, SAXS is a more reliable technique because NPs can overlap in HPS (Figure 2a,b),

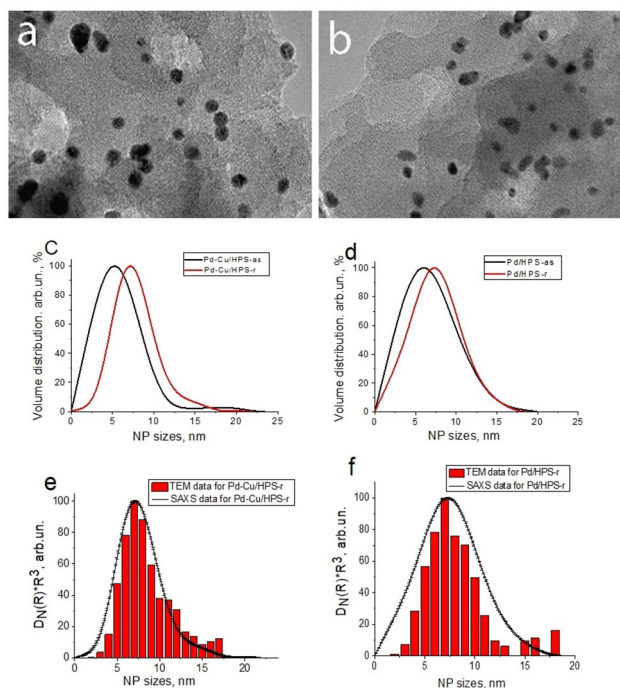


Figure 2. TEM images (a,b), volume NP size distribution from the SAXS data (c,d), and a comparison of the NP sizes from TEM and SAXS data (e,f) for Pd–Cu/HPS-r (a,c,e) and Pd/HPS-r (b,d,f).

giving irregular, non-spherical projections and making the NP size evaluation untrustworthy, unless very high NP populations are examined for better fidelity. On the other hand, in some cases SAXS data can result in the NP size overestimation.^[16] Thus, the combination of both techniques is the most trustworthy approach. The NP diameter distributions obtained by measuring 709 NPs for Pd–Cu/HPS-r and 841 NPs for Pd/HPS-r on the respective TEM images are shown in Figure S2. The experimental SAXS data and the best fits for spherical NPs are presented in Figure S3. The radii of gyration and NP diameters are shown in Table S4.

For both bimetallic (Pd–Cu) and monometallic (Pd) samples (Figure 2c, d), as-synthesized NPs are smaller than those after the hydrogen reduction. The increase of NP sizes upon reduction indicates that there is a migration of metal species between NPs, i.e., ripening, which is not surprising due to an elevated reduction temperature (275 °C). The NP sizes obtained from TEM and SAXS data are in good agreement, especially for bimetallic NPs. The mean NP size from both methods is about 6–7 nm which noticeably exceeds the typical pore size (4 nm) (Figure S4). This reveals that NPs are mainly located in pore junctions, but without blocking the pore system as about ~60% of pore volume remains available.

The X-ray diffraction (XRD) patterns of Pd–Cu/HPS-r and Pd/HPS-r and their high resolution (HR) X-ray photoelectron spectroscopy (XPS) Pd3d spectra are presented in Figure 3.

The XRD pattern of Pd/HPS-r shows typical reflections of Pd⁰ (JCPDS-ICDD 46-1043), whose line broadening allowed us to determine the crystallite size of 6 nm, indicating that Pd NPs are most likely single crystals. For bimetallic Pd–Cu NPs in Pd–Cu/

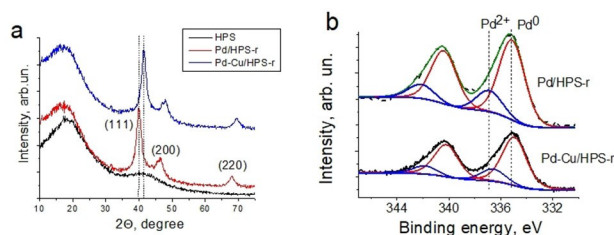


Figure 3. XRD patterns (a) of Pd–Cu/HPS-r and Pd/HPS-r and their HR XPS Pd3d spectra (b).

HPS-r, the XRD pattern is nearly identical, but its reflections are shifted towards larger angles and the peak positions are in between those characteristic of Pd (JCPDS-ICDD 46-1043) and Cu (JCPDS-ICDD 4-9-2090) phases. According to the literature data,^[17] this peak positioning reveals the formation of the bimetallic Pd–Cu alloy. The absence of the reflections from Cu metal as well as its oxides or hydroxides once more confirms the alloy formation. The crystallite size of Pd–Cu alloy NPs is also ~6 nm which could be underestimation due to NP heterogeneity. It is worth noting that as-synthesized mono- and bimetallic samples are completely amorphous and their XRD patterns (not shown) resemble that of HPS. This was anticipated, considering mild conditions of the sample preparation (70 °C). Thus, the hydrogen treatment (at 275 °C) of a mixed Pd–Cu oxide is accompanied by metal reduction and crystallization. According to Vegard's rule, ideal Pd–Cu alloys should show a linear increase of lattice parameters with the Pd content increase.^[18] In the case of Pd–Cu/HPS-r (37 at.% Pd by elemental analysis), the calculated lattice parameter should be 3.75 Å, while in fact, it is 3.87 Å, revealing heterogeneity of alloy NPs,^[19] which is further revealed by XPS.

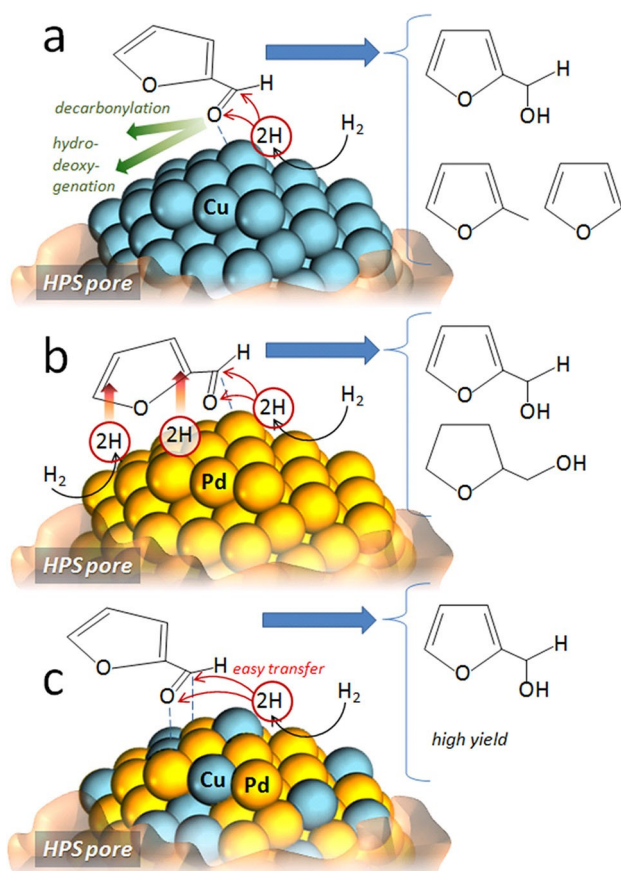
For both samples, the deconvolution of the HR XPS Pd3d spectra results in two doublets in the Pd3d_{5/2} and Pd3d_{3/2} regions. The Pd3d_{5/2} peak positions at 335.0–335.1 eV and 336.5–336.9 eV (Table S5) are typical for Pd⁰ and Pd²⁺ (most likely PdO),^[20] respectively, with nearly the same Pd⁰:Pd²⁺ ratios (Table S5). The HR XPS Cu2p spectrum of Pd–Cu/HPS-r (Figure S5) shows that the major component is Cu⁰ with a smaller fraction of Cu²⁺ (Table S6). The BE of Cu⁰ (932.2 eV) is typical for Cu NPs.^[21] The presence of Cu²⁺ could be due to incomplete reduction of CuO in the as-synthesized sample or oxidation of Cu⁰ species under air. A comparison of the Pd:Cu atomic ratio from XPS (surface method) and the elemental analysis data (bulk method) demonstrate an enrichment of the NP surface by copper, i.e., heterogeneity. Both theory and experiment demonstrate that the metal with the lowest surface energy has a tendency to segregate to the surface of alloys.^[22] In our case, Cu with the average surface energy of 113.9 meVÅ^{–2} favors the surface enrichment compared to Pd, whose average surface energy is 131 meVÅ^{–2}.^[22] Nonetheless, XRD demonstrates the formation of Pd–Cu alloy which enhances interactions between Pd and Cu atoms,^[23] boosting the NP catalytic performance.

Influence of Pd-Cu interactions in alloy NPs on the catalytic action

To evaluate the influence of Pd–Cu interactions in Pd–Cu/HPS-r on the selective hydrogenation of FF to FA, we assessed the functions of Cu and Pd in monometallic catalysts. The data presented in Table S2 demonstrate that for all Cu/HPS catalysts, the FF hydrogenation products are FA, furan, and 2-methylfuran (Scheme 2a). This is in agreement with the literature data,^[5a] indicating that copper based catalysts facilitate hydrogenation of the C=O bond due its adsorption on the catalytic site, while the C=C bonds in the furan ring remain unchanged.^[1c,4c,5a,10a]

Alternatively, for Pd/HPS catalysts (Table S2), the FF hydrogenation products are only FA and THFA,^[9c] revealing that on the Pd surface both the C=O group and the furan ring are adsorbed due to planarity of the FF molecule. The C=C bonds interact with Pd via π - π interactions (Scheme 2b).^[5a,14a]

It was demonstrated that when two metals, Cu and Pd, are combined in a bimetallic NP, the NP surface properties as well as the structure of active sites change, thus, affecting the chemical reactivity, which could be assigned to weaker interactions between metal sites and FA (for easy desorption).^[6c,9c] This is well illustrated for Pd–Cu alloy NPs in Pd–Cu/HPS-r, allowing for 99.9% of the FF conversion and the 95.2% selectivity to FA (Table 1). To the best of our knowledge,



Scheme 2. Schematic representation of FF hydrogenation on Cu (a), Pd (b), and Pd–Cu NPs.

this is one of the highest values of the FA selectivity at the 100% FF conversion, reported to date.^[14] Although a higher selectivity (98.6%) has been described for Pd–Cu/MgO,^[9c] a double catalyst amount was required in that case. The presence of Cu in bimetallic NPs most probably disrupts the weaker C=C bond adsorption on neighboring Pd atoms, leading to the higher yield of the target product. However, the question arises what degree of disruption is needed and what electronic state of metal species is favored?

It was established that a combination of Pd and Cu may change the electronic structure of Pd species compared to pure Pd, decreasing the decarbonylation rate, while increasing the hydrogenation rate.^[14a] In the reaction mechanism study of bimetallic Pd–Cu NPs, it was discovered that the presence of Cu improves the selectivity to FA, while Pd mainly increases the FF conversion most likely due to optimized hydrogen adsorption (Scheme 2c),^[14b] preventing hydrogen oversaturation on the surface and allowing for the better FF adsorption.^[11a] Moreover, for dissociative hydrogen adsorption on metal, the presence of zerovalent and cationic metal species is essential.^[9c,14b] The data presented in Tables S5 and S6 demonstrate that in Pd–Cu alloy NPs (the Pd–Cu/HPS-r sample), both Pd⁰–Pd²⁺ and Cu⁰–Cu²⁺ pairs exist with approximately 20% of oxidized species. This distribution of oxidized-reduced Pd–Cu species seems to be beneficial for optimal hydrogen adsorption and high FF conversion, while the disruption of Pd atom coverage on the NP surface due to alloying and enrichment by Cu (Table S6) may lead to suppression of the furan ring adsorption and its hydrogenation, thus, high FA selectivity. The TOF value for Pd–Cu/HPS-r, calculated per moles of NP surface atoms (taking into account Pd:Cu ratios on the surface and in bulk, Table S6) is 1209 h⁻¹, which is comparable (1148 h⁻¹ in ref. [24]) or exceeds the values reported for many other heterogeneous catalytic systems, for example 204 h⁻¹ in ref. [25], 21 h⁻¹ in ref. [26], 96 h⁻¹ in ref. [10b], ~400 h⁻¹ in ref. [27], 952 h⁻¹ in ref. [28], etc. The only exception is a customised catalytic membrane reactor with the Ru-polyethersulfone membrane, allowing TOF of 48000 h⁻¹,^[3b] but a special equipment is required in this case and the conversion is only 26.13%.

In view of high conversion and selectivity of Pd–Cu/HPS-r, we studied reusability of this catalyst in ten consecutive reactions. Figure 4 demonstrates that both conversion and selectivity to FA decrease by only a couple of percent after ten cycles, indicating enhanced stability of alloy NPs in the HPS pores as well as practically unchanged catalytic performance which exceeds the catalytic performance upon reusability of other catalysts.^[9c,10a]

Conclusion

We developed a novel catalyst for the selective FF hydrogenation based on Pd–Cu alloy NPs and the commercially available micro/mesoporous HPS support. The advantages of this inexpensive polymer support such as high porosity and mechanical robustness, were fully realized by forming well-defined 6–7 nm NPs in the pore junctions, providing a sufficient

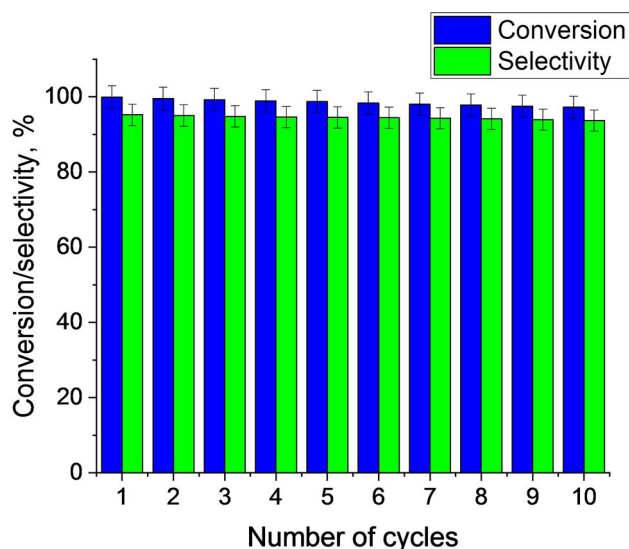


Figure 4. Conversion and selectivity to FA in repeated uses of Pd–Cu/HPS-r. The reaction time for all reuse experiments remained 180 min.

pore system (~60% by volume) for transport of reacting and target molecules. XRD confirmed the formation of alloy Pd–Cu NPs, while XPS showed the enrichment of the NP surface with Cu atoms as well as the presence of both zerovalent and cationic Pd and Cu species, i.e., NP heterogeneity. Such a structure of Pd–Cu alloy NPs allowed for nearly 100% conversion and excellent selectivity to FA (95.2%) along with a significant activity of the catalyst ($\text{TOF}_3 = 1209 \text{ h}^{-1}$). This exceptional performance was attributed to the prevention of the furan ring adsorption on Pd due to neighboring Cu species and facilitated FA desorption, both leading to higher selectivity. Controlled hydrogen and FF adsorption due to mixed valence states of Pd and Cu species lead to higher conversion. These factors as well as remarkable catalyst reusability in ten consecutive reactions makes this catalyst promising for practical applications.

Experimental Section

The description of materials, analysis of catalytic samples, and characterization methods are presented in the Supporting Information.

Synthesis of catalysts

The Pd–Cu-containing HPS-based catalyst was synthesized via a wet-impregnation method according to the procedure described elsewhere for Pd/HPS using Pd acetate as precursor.^[2a] In a typical experiment, 1 g of HPS granules (pretreated, dried and crushed to the size $< 60 \mu\text{m}$) were impregnated with 3 mL of THF solution containing 0.071 g of $\text{Pd}(\text{CH}_3\text{COO})_2$ and 0.090 g of $\text{Cu}(\text{CH}_3\text{COO})_2 \times \text{H}_2\text{O}$. The product was dried at 70°C for 1 h and treated with 2.7 mL of the 0.3 M Na_2CO_3 solution for precipitation of oxides/hydroxide NPs.^[6b,14b]

After that the catalyst was washed with distilled water until neutral pH and dried at 70°C for 2 h. The catalyst was denoted “as-

synthesized” (as). Reduction of Pd and Cu species in the catalyst was carried out in a hydrogen flow at 275°C for 2 h. The catalyst was denoted “reduced” (r). Monometallic Cu- and Pd-containing catalysts were prepared in a similar way using a single precursor.

Catalytic testing

FF hydrogenation was performed in a Parr reactor (Series 5000 Multiple Reactor, stainless steel). In a typical experiment, the catalyst (0.1 g) was mixed with 24 mL of isopropanol and treated in a hydrogen flow for 30 min at 120°C and 6.0 MPa pressure under vigorous stirring (1000 rpm) for the catalyst activation. After that 2 mL of FF and another 24 mL of isopropanol were added to the reactor. Samples of the reaction mixture were taken for analysis regularly and analyzed with GC-MS (Shimadzu GCMS-QP2010S) equipped with a capillary column HP-1MS (30 m \times 0.25 mm i.d., 0.25 μm film thickness) (see details in the Supporting Information). The experiments were performed for 180 min. The TOF value for Pd–Cu/HPS-r was calculated as moles of the substrate consumed per moles of NP surface atoms (calculated knowing the NP size and composition) per hour.

For reusability experiments, the reaction mixture was placed in glass tubes and the catalyst was separated by centrifugation using a bench centrifuge at 4,000 rpm. The supernatant was removed and the catalyst was washed with isopropanol three times, following the same isolation procedure. Finally, the catalyst was utilized in the repeated experiments without drying.

Acknowledgements

The research leading to these results has received funding from the Russian Science Foundation (project 19-19-00490), supporting physicochemical studies and the manuscript preparation. K.S. and A.S. thank the Russian Foundation for Basic Research, which supported catalytic testing (grant 19-38-90049) and studies of the catalyst reuse (grant 20-08-00433). Y.L. acknowledges the resource center “VTAN” (Novosibirsk State University) for the access to instrumentation.

Conflict of Interest

The authors declare no conflict of interest.

Keywords: furfural · hydrogenation · hypercrosslinked polystyrene · nanostructures · Pd–Cu alloys

- [1] a) P. Liu, W. Qiu, C. Zhang, Q. Tan, C. Zhang, W. Zhang, Y. Song, H. Wang, C. Li, *ChemCatChem* **2019**, *11*, 3296–3306; b) J.-P. Lange, E. van der Heide, J. van Buijtenen, R. Price, *ChemSusChem* **2012**, *5*, 150–166; c) K. Gupta, R. K. Rai, S. K. Singh, *ChemCatChem* **2018**, *10*, 2326–2349; d) X. Li, P. Jia, T. Wang, *ACS Catal.* **2016**, *6*, 7621–7640; e) J. Parikh, S. Srivastava, G. C. Jadeja, *Ind. Eng. Chem. Res.* **2019**, *58*, 16138–16152; f) D. Vargas-Hernandez, J. M. Rubio-Caballero, R. Moreno-Tost, J. M. Merida-Robles, J. Santamaria-Gonzalez, A. Jimenez-Lopez, M. A. Perez-Cruz, R. Hernandez-Huesca, P. Maireles-Torres, *Mod. Res. Catal.* **2016**, *5*, 85–94.
- [2] a) K. E. Salnikova, V. G. Matveeva, Y. V. Larichev, A. V. Bykov, G. N. Demidenko, I. P. Shkileva, M. G. Sulman, *Catal. Today* **2019**, *329*, 142–148; b) Z. Yi, H. Xu, D. Hu, K. Yan, *J. Alloys Compd.* **2019**, *799*, 59–65.

- [3] a) A. Corma, S. Iborra, A. Velty, *Chem. Rev.* **2007**, *107*, 2411–2502; b) G. Bagnato, A. Figoli, C. Ursino, F. Galiano, A. Sanna, *J. Mater. Chem. A* **2018**, *6*, 4955–4965.
- [4] a) C. Nguyen-Huy, H. Lee, J. Lee, J. H. Kwak, K. An, *Appl. Catal. A* **2019**, *571*, 118–126; b) Y. Nakagawa, M. Tamura, K. Tomishige, *ACS Catal.* **2013**, *3*, 2655–2668; c) S. Chen, R. Wojcieszak, F. Dumeignil, E. Marceau, S. Royer, *Chem. Rev.* **2018**, *118*, 11023–11117.
- [5] a) S. Sitthisa, D. E. Resasco, *Catal. Lett.* **2011**, *141*, 784–791; b) C. Li, G. Xu, X. Liu, Y. Zhang, Y. Fu, *Ind. Eng. Chem. Res.* **2017**, *56*, 8843–8849; c) J. Lee, J. Woo, C. Nguyen-Huy, M. S. Lee, S. H. Joo, K. An, *Catal. Today* **2020**, *350*, 71–79.
- [6] a) R. Kosydar, D. Duraczynska, J. Gurgul, J. Krysiak-Czerwenka, A. Drelinkiewicz, *React. Kinet. Mech. Catal.* **2019**, *126*, 417–437; b) R. M. Mironenko, V. P. Talsi, T. I. Gulyaeva, M. V. Trenikhin, O. B. Belskaya, *React. Kinet. Mech. Catal.* **2019**, *126*, 811–827; c) M. Hronec, K. Fulajtarova, I. Vavra, T. Sotak, E. Dobrocka, M. Micusik, *Appl. Catal. B* **2016**, *181*, 210–219.
- [7] a) N. Cherkasov, V. Jadvani, J. Mann, Y. B. Losovyj, Z. B. Shifrina, L. M. Bronstein, E. V. Rebrov, *Fuel Process. Technol.* **2017**, *167*, 738–746; b) Y. Wang, Y. S. Lin, *J. Sol-Gel Sci. Technol.* **1998**, *11*, 185–195.
- [8] a) Z. B. Shifrina, V. G. Matveeva, L. M. Bronstein, *Chem. Rev.* **2020**, *120*, 1350–1396; b) J. Huang, S. R. Turner, *Polym. Rev.* **2018**, *58*, 1–41.
- [9] a) N. Pino, S. Sitthisa, Q. Tan, T. Souza, D. Lopez, D. E. Resasco, *J. Catal.* **2017**, *350*, 30–40; b) Y. Nakagawa, K. Takada, M. Tamura, K. Tomishige, *ACS Catal.* **2014**, *4*, 2718–2726; c) K. Fulajtarova, T. Sotak, M. Hronec, I. Vavra, E. Dobrocka, M. Omastova, *Appl. Catal. A* **2015**, *502*, 78–85; d) N. Cherkasov, A. J. Exposito, M. S. Aw, J. Fernandez-Garcia, S. Huband, J. Sloan, L. Paniwnyk, E. V. Rebrov, *Appl. Catal. A* **2019**, *570*, 183–191.
- [10] a) H. Du, X. Ma, P. Yan, M. Jiang, Z. Zhao, Z. C. Zhang, *Fuel Process. Technol.* **2019**, *193*, 221–231; b) M. Lesiak, M. Binczarski, S. Karski, W. Maniukiewicz, J. Rogowski, E. Szubiakiewicz, J. Berlowska, P. Dziugan, I. Witonska, *J. Mol. Catal. A* **2014**, *395*, 337–348.
- [11] a) V. G. Matveeva, E. M. Sulman, O. V. Manaenkov, A. E. Filatova, O. V. Kislitza, A. I. Sidorov, V. Y. Doluda, M. G. Sulman, E. V. Rebrov, *Catal. Today* **2017**, *280*, 45–50; b) V. N. Sapunov, M. Y. Grigoryev, E. M. Sulman, M. B. Konyaeva, V. G. Matveeva, *J. Phys. Chem. A* **2013**, *117*, 4073–4083.
- [12] J.-Y. Luo, M. Meng, J.-S. Yao, X.-G. Li, Y.-Q. Zha, X. Wang, T.-Y. Zhang, *Appl. Catal. B* **2009**, *87*, 92–103.
- [13] C. J. Barrett, J. N. Chheda, G. W. Huber, J. A. Dumesic, *Appl. Catal. B* **2006**, *66*, 111–118.
- [14] a) S. Sitthisa, T. Pham, T. Prasomsri, T. Sooknoi, R. G. Mallinson, D. E. Resasco, *J. Catal.* **2011**, *280*, 17–27; b) J. Du, J. Zhang, Y. Sun, W. Jia, Z. Si, H. Gao, X. Tang, X. Zeng, T. Lei, S. Liu, L. Lin, *J. Catal.* **2018**, *368*, 69–78.
- [15] M. G. Schwab, I. Senkova, M. Rose, N. Klein, M. Koch, J. Pahnke, G. Jonschker, B. Schmitz, M. Hirscher, S. Kaskel, *Soft Matter* **2009**, *5*, 1055–1059.
- [16] T. Li, A. J. Senesi, B. Lee, *Chem. Rev.* **2016**, *116*, 11128–11180.
- [17] G. Behmenyar, A. N. Akin, *J. Power Sources* **2014**, *249*, 239–246.
- [18] A. Peles, M. Shao, L. Protsailo, *Catalysts* **2015**, *5*, 1193–1201.
- [19] T. Kawaguchi, W. Cha, V. Latyshev, S. Vorobiov, V. Komanicky, H. You, *arXiv.org, e-Print Arch., Condens. Matter* **2019**, 1–14.
- [20] a) L. Gregor, A. K. Reilly, T. A. Dickstein, S. Mazhar, S. Bram, D. G. Morgan, Y. Losovyj, M. Pink, B. D. Stein, V. G. Matveeva, L. M. Bronstein, *ACS Omega* **2018**, *3*, 14717–14725; b) M. Brun, A. Berther, J. C. Bertolini, *J. Electron Spectrosc. Relat. Phenom.* **1999**, *104*, 55–60.
- [21] a) T. Kruk, K. Szczepanowicz, J. Stefanska, R. P. Socha, P. Warszynski, *Colloids Surf. B* **2015**, *128*, 17–22; b) Y. Song, D. Cho, S. Venkateswarlu, M. Yoon, *RSC Adv.* **2017**, *7*, 10592–10600; c) Y. Bai, Q. Wang, C. Du, T. Bu, Y. Liu, X. Sun, W. Luo, R. Li, Y. Zhao, X. Zheng, L. Wang, *J. Colloid Interface Sci.* **2019**, *553*, 768–777.
- [22] R. Ferrando, J. Jellinek, R. L. Johnston, *Chem. Rev.* **2008**, *108*, 845–910.
- [23] B. T. Meshesha, N. Barrabes, J. Llorca, A. Dafinov, F. Medina, K. Foettinger, *Appl. Catal. A* **2013**, *453*, 130–141.
- [24] G. Wang, R. Yao, H. Xin, Y. Guan, P. Wu, X. Li, *RSC Adv.* **2018**, *8*, 37243–37253.
- [25] C. K. P. Neeli, Y.-M. Chung, W.-S. Ahn, *ChemCatChem* **2017**, *9*, 4570–4579.
- [26] Y. Feng, G. Yan, T. Wang, W. Jia, X. Zeng, J. Sperry, Y. Sun, X. Tang, T. Lei, L. Lin, *Green Chem.* **2019**, *21*, 4319–4323.
- [27] M. Li, L. Collado, F. Cardenas-Lizana, M. A. Keane, *Catal. Lett.* **2018**, *148*, 90–96.
- [28] W. S. Putro, T. Kojima, T. Hara, N. Ichikuni, S. Shimazu, *Catal. Sci. Technol.* **2017**, *7*, 3637–3646.

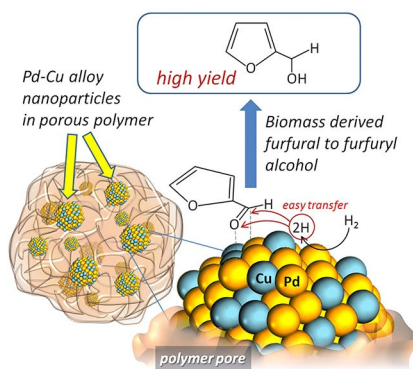
Manuscript received: May 14, 2020

Revised manuscript received: June 26, 2020

Accepted manuscript online: June 29, 2020

FULL PAPERS

Biomass-derived furfural hydrogenation: Pd–Cu alloy nanoparticles (NPs) were prepared in pores of inexpensive, commercially available hypercrosslinked polystyrene (HPS) and were tested in selective furfural (FF) hydrogenation to furfuryl alcohol (FA). The controlled surface composition of Pd–Cu NPs ensures high FF conversion and FA selectivity, while the NP location in HPS pores allows for high stability upon reuse in ten consecutive reactions.



K. E. Salnikova, Dr. Y. V. Larichev, Prof. E. M. Sulman, Dr. A. V. Bykov, Dr. A. I. Sidorov, Dr. G. N. Demidenko, Prof. M. G. Sulman, Dr. L. M. Bronstein, Prof. V. G. Matveeva**

1 – 8

Selective Hydrogenation of Biomass-Derived Furfural: Enhanced Catalytic Performance of Pd–Cu Alloy Nanoparticles in Porous Polymer

